



Evidence of excess oxygen accommodation in yttria partially-stabilized zirconia

Simon C. Middleburgh^{a,*}, Iuliia Ipatova^a, Lee J. Evitts^a, Michael J.D. Rushton^a, Ben Assinder^b, Robin W. Grimes^c, William E. Lee^{a,c}

^a Nuclear Futures Institute, Bangor University, Bangor LL57 1UT, United Kingdom

^b School of Electronic Engineering, Bangor University, LL57 1UT, United Kingdom

^c Department of Materials, Imperial College London, London, SW7 2AZ, United Kingdom

ARTICLE INFO

Article history:

Received 24 July 2019

Received in revised form 19 August 2019

Accepted 30 August 2019

Available online xxx

Keywords:

Non-stoichiometry

Yttria partially stabilized zirconia

Raman spectroscopy

Density functional theory

Peroxide ion defect

ABSTRACT

Yttria partially stabilized zirconia (ZrO_2)_x(Y_2O_3)_{1-x} has been investigated to understand accommodation of excess oxygen into its structure. ZrO_2 powder with 8 wt% Y_2O_3 additions was treated in 30 vol% H_2O_2 solution to promote oxidation of the material. A new Raman peak was observed after treatment at 840 cm^{-1} , consistent with previous reports of solid state peroxide ions (O_2^{2-}). This was corroborated using atomic scale simulation based on density functional theory; these also highlighted the near-zero solution enthalpy for excess oxygen in the monoclinic structure via the formation of a peroxide ion defect.

© 2019 Published by Elsevier Ltd on behalf of Acta Materialia Inc.

Zirconia is an oxide widely used in both structural and functional roles. This refractory material exhibits relatively high toughness and oxidation resistance, making it suitable in applications ranging from cutting tools [1], bone prostheses [2] to thermal barrier coatings [3]. Its high ionic conductivity has led to its widespread use as an oxygen sensor in automobile emissions systems and as an electrolyte in solid-oxide fuel-cells [4].

Zirconia has complex polymorphism with cubic, tetragonal, orthorhombic and monoclinic structures readily observed. Under standard conditions, pure ZrO_2 has the monoclinic structure, however, the tetragonal or cubic polymorph can be stabilized down to room temperature by adding one of several oxides in various concentrations, including CaO , MgO , CeO_2 and Y_2O_3 . This is revealed by the enlargement of the tetragonal and/or cubic phase field in the binary phase diagrams [5]. Of these binary systems yttria stabilized zirconia is perhaps the most well studied [6].

Yttria enters solution within the zirconia lattice by creating charge compensating defects [7]. Yttrium ions have a formal charge of $3+$ whilst zirconium ions have a formal charge of $4+$. Substitution of Y^{3+} onto a Zr^{4+} site requires a positively charged defect. This charge compensating defect is reported to be half an oxygen vacancy, which can lead to the formation of the $\{2\text{Y}_{\text{Zr}}'\text{V}_{\text{O}}^{\bullet}\}^{\times}$ neutral defect cluster [7]. The presence of oxygen vacancies improves the ionic conductivity of

the material – with peak conductivity occurring at approximately 10 at.% Y_2O_3 additions to ZrO_2 providing ionic conductivities similar to other leading fuel cell oxides including CGO ($\text{Ce}_{0.9}\text{Gd}_{0.1}\text{O}_{1.95}$) and BICUVOX.10 ($\text{Bi}_2\text{V}_{1.9}\text{Cu}_{0.1}\text{O}_{5.35}$) [8].

Stoichiometry in these ionically-conducting systems is of paramount importance. Deviations could be detrimental to their behaviour whether used as solid electrolytes, thermal barrier coatings or as other functional components. Past work has found that in oxides with cations that are not readily oxidized (e.g. Zr^{4+} to Zr^{5+}), the oxygen itself can oxidize to accommodate oxygen, in the case of zirconate perovskites [9] and some fluorite structures [10] this oxidation is accommodated through the formation of a neutral peroxide ion defect (O_2^{2-}). Peroxide ions form readily in group II monoxides [11,12] and theoretical work has been carried out to understand how stoichiometry can vary in amorphous ZrO_2 compared to its crystalline forms – predicting that additional oxygen can be readily accommodated in the amorphous phase [13].

In this paper the accommodation of excess oxygen into solid solutions of ZrO_2 and Y_2O_3 is investigated both theoretically and experimentally. Commercially available ZrO_2 with 8 wt% Y_2O_3 (YSZ-8) is analysed using X-ray diffraction and Raman spectroscopy before and after treatment with H_2O_2 solution. DFT based calculations were subsequently conducted consistent with the experimental studies, which shed light on how excess oxygen may be incorporated.

YSZ-8 was obtained from Merck (product number 544779) as a powder with particle size $<100\text{ nm}$. Room temperature X-ray diffraction

* Corresponding author.

E-mail address: s.middleburgh@bangor.ac.uk (S.C. Middleburgh).

patterns of the as received material were obtained using a PANalytical Aeris X-ray diffractometer with Cu-K α radiation ($\lambda = 1.5406 \text{ \AA}$, voltage = 40 kV and current = 7.5 mA) and are reported in Fig. 1. Scans were taken in the 2θ range 10° to 80° at increments of 0.01° with a time-step of 60s. The X-ray diffraction (XRD) analysis of the as-received YSZ-8 sample demonstrates the existence of two crystalline phases: primarily a tetragonal phase (60%) with the remainder made up of the monoclinic phase (using the same methodology for crystal phase identification first used by Toraya et al. [14]), consistent with previous examinations of this compound [15,16,17]. A finer X-ray diffraction pattern was obtained on the same material between 72 and 76° to verify the c/a ratio of the tetragonal phase in order to identify its nature (either the equilibrium phase or the metastable form). Two peaks were observed in this range at 73.13° and 74.35° , identified as the (004) and (220) peaks of the tetragonal phase [18] giving lattice parameters of $a = b = 3.607 \text{ \AA}$ and $c = 5.173 \text{ \AA}$. This gives a $a/\sqrt{2}$ of 1.014, indicating that the tetragonal phase resides within the transformable tetragonal phase as described by Viazzi et al. [18] which also corresponds to a $\text{YO}_{1.5}$ content of 6.4 mol%.

The as-received material was heated to 1200°C for 2 h and then rapidly cooled in air back to room temperature. The resulting X-ray diffraction pattern showed a marked increase of the tetragonal phase to 95% (the remainder being monoclinic). The peak positions between 72 and 76° did not shift, as is expected in the non-equilibrium phase diagram according to Chevalier and Gremillard [19] and Fabrichnaya and Aldinger [20].

To understand the potential for excess oxygen accommodation, the powder was treated in 30 vol% H_2O_2 solution for 1 day and 1 week at 5°C before rinsing in deionized water and drying on filter paper for 24 h at room temperature (similar to [9]).

Raman spectra were obtained using a Bruker Senterra 2 instrument equipped with a 532 nm laser. The laser power was 25 mW and a $50 \mu\text{m}$ aperture was used. An integration time of 5 s was applied with 5 co-additions. The stated spectral resolution was 4 cm^{-1} . Raman spectroscopy was performed on two sets of samples: the as-received YSZ-8 sample and the heated sample in dry, wet treated (straight after 30 vol% H_2O_2 treatment) and dry treated states.

The Raman spectra for the three states of the as-received material and the material treated for 1 week are shown in Fig. 2. Raman peaks for both the monoclinic and tetragonal phases of PTZ are consistent with previous studies [19,20,21] (and are highlighted in Fig. 2). There were no observed changes in the characteristic peaks between the samples, with both tetragonal and monoclinic peaks being discernible and analysis using the methodology of [21] indicating a tetragonal phase composition of 55%.

A large peak at 876 cm^{-1} was observed in the wet, treated sample which is consistent with the O—O stretching mode in hydrogen peroxide solution [22,23]. A peak remains at 840 cm^{-1} in the dried sample

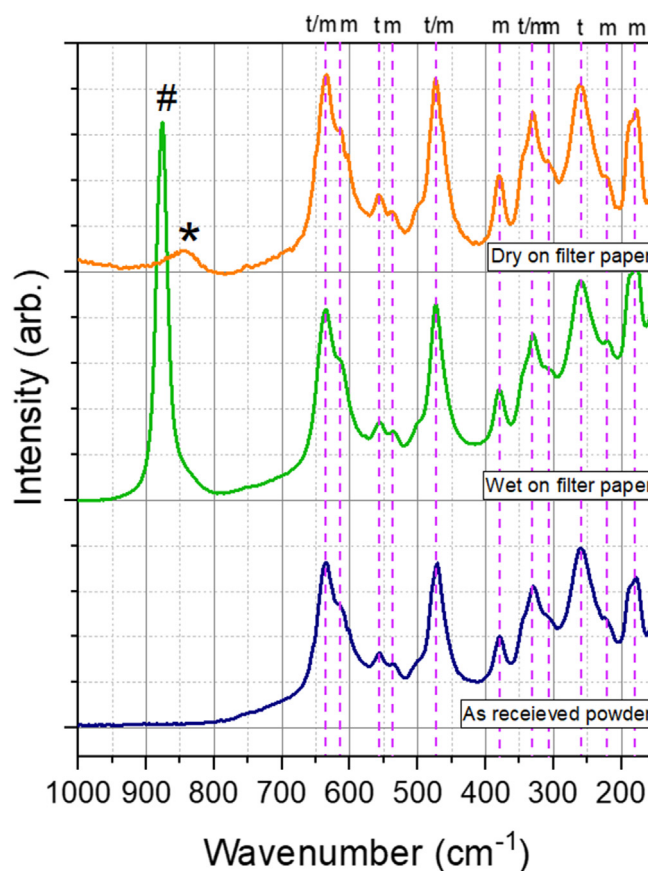


Fig. 2. Raman spectra for the as-received YSZ-8 untreated sample, during treatment with 30 vol% H_2O_2 and following treatment and drying. The characteristic peaks for the monoclinic (m) and tetragonal (t) phases of ZrO_2 [20] are highlighted in addition to two extra peaks associated with the H_2O_2 in solution (# at 876 cm^{-1}) and an extra peak observed after drying the sample (* at 840 cm^{-1}).

that was not present in the original sample (a smaller peak in this position was also evident in the sample removed from H_2O_2 solution after 1 day). This 840 cm^{-1} peak is consistent with the O—O peroxide ion stretching mode reported in previous work in MgO and Mg/BaO catalysis material reported by Lunsford et al. [11] as well as Su and Bell [12]. Additionally, the 840 cm^{-1} peak is consistent with the peroxide ion observed in BeO using similar sample preparation techniques to those used in this study [24]. The peak at 840 cm^{-1} was still evident after four weeks (stored at room temperature in a desiccator). The peak height had diminished to approximately half of the 24 h dried sample. The peak was not apparent after heat treatment of the sample at 200°C for 2 h.

The YSZ-8 material that was heat treated to 1200°C was analysed in a similar manner to the as-received material. Only tetragonal peaks were observed in the pre-treated sample. After treatment in the hydrogen peroxide solution, the peak at 876 cm^{-1} was observed in the wet sample, but upon drying, no additional peaks were observed when compared to the pre-treated sample (indicating that the mode affiliated with the additional peak in the non-heat treated sample is associated with the monoclinic phase).

To further investigate the potential for peroxide ion formation in YSZ-8, DFT calculations were performed with the Vienna Ab-initio Simulation Package (VASP) [25–28]. The projector augmented wave (PAW) [29,30] library supplied with the software was used with a GGA exchange correlation functional described by Perdew, Burke and Ernzerhof [31,32]. The cut-off energy was set at 500 eV for all calculations with a Gaussian smearing width of 0.1 eV. The self-consistent field (SCF) stopping criterion was set to $1 \times 10^{-4} \text{ eV}$ and the geometry optimization stopping criterion was set at $1 \times 10^{-3} \text{ eV}$. Atomic positions

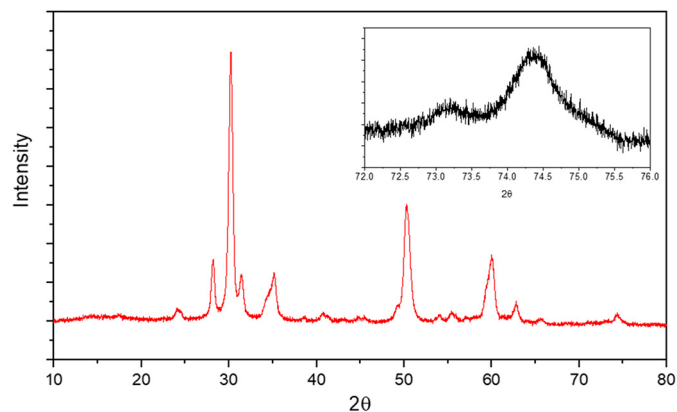
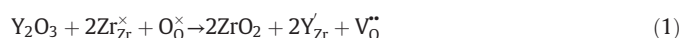


Fig. 1. X-ray diffraction pattern for the as-received YSZ-8 material. Inset shows detailed X-ray diffraction pattern between 72 and 76° 2θ .

and simulation cell vectors were all free to relax during energy minimisation unless stated. In all calculations, a gamma-centred $4 \times 4 \times 4$ k-point grid was set automatically using the Monkhorst-Pack scheme. Monoclinic and tetragonal polymorphs of ZrO_2 doped with Y_2O_3 were considered – each with 32 cation sites and 64 oxygen sites. Two Y atoms were substituted onto two Zr sites in each supercell (producing a 6.25 mol% composition – a good comparison to the experimental material) and charge compensated through the formation of an oxygen vacancy in a ratio of 2:1 to maintain charge neutrality forming the $\{2\text{Y}_{\text{Zr}}':\text{V}_{\text{O}}^{\bullet\bullet}\}^{\times}$ cluster. The arrangement of the defect cluster is considered in a similar manner to previous studies [7,33,34].

The solution energy of Y_2O_3 into the monoclinic and tetragonal phases was first assessed in order to identify the lowest energy arrangement of the $\{2\text{Y}_{\text{Zr}}':\text{V}_{\text{O}}^{\bullet\bullet}\}^{\times}$ cluster in the tetragonal and monoclinic structures. The Y substitutional species were most stable when in a second nearest neighbour position to the oxygen vacancy whilst being at a maximum separation from each-other, similar to previous atomic scale studies [7,35]. Solution of Y_2O_3 into monoclinic and tetragonal polymorphs is predicted to proceed with energies of 1.79 eV and 1.09 eV, respectively, via the following reaction (using Kröger-Vink notation [36]):



This calculated reduction in solution enthalpy in forming a tetragonal phase highlights the stabilizing effect that substituting Y has in the ZrO_2 system.

Further calculations were performed to investigate accommodation of an extra oxygen atom into the Y-containing monoclinic and tetragonal polymorphs of ZrO_2 . The additional oxygen was placed directly onto the charge balancing vacancy site. After relaxation, a configuration consistent with the peroxide ion defect formed through the lattice relaxation procedure. To gauge the propensity for oxygen to enter the monoclinic or tetragonal structures, solution was considered from molecular oxygen. The solution enthalpy was computed to be -0.03 eV and 0.79 eV in the monoclinic and tetragonal structures containing the $\{2\text{Y}_{\text{Zr}}':\text{V}_{\text{O}}^{\bullet\bullet}\}^{\times}$ defect cluster, respectively. The O–O bond distances associated with the defect were 1.49 Å and 1.48 Å in the monoclinic and tetragonal structures: consistent with the peroxide ion (O_2^{2-}) [37].

The near-zero solution enthalpy of O_2 into monoclinic ZrO_2 containing $\{2\text{Y}_{\text{Zr}}':\text{V}_{\text{O}}^{\bullet\bullet}\}^{\times}$, as well as the low energy computed for solution into the tetragonal structure indicates that the stoichiometry in the $(\text{ZrO}_2)_{1-x}(\text{Y}_2\text{O}_3)_x$ system can vary, depending on the polymorph present and composition of the $(\text{ZrO}_2)_{1-x}(\text{Y}_2\text{O}_3)_x$. The preference for oxygen accommodation in the monoclinic phase echoes the experimental observation that the peak at 840 cm^{-1} was only observed in the sample with a significant monoclinic phase fraction.

To calculate the vibrational wavenumber associated with the additional oxygen defect cluster (the neutral O_2^{2-} peroxide ion), the cluster was compressed and stretched along its axis in increments of 1.25% . The spring constant was calculated by taking the derivative of the energy-distance function. The wavenumber was then determined from the spring constant via [9]:

$$\nu = \left(\frac{k(2m)}{4\pi^2 c^2 m^2} \right)^{\frac{1}{2}} \quad (2)$$

where k is the spring constant in N/cm^2 , m is the mass of an oxygen atom in kg, and c is the speed of light in cm/s .

The wavenumbers associated with the O–O stretching mode, calculated in both the monoclinic and tetragonal structures, were 851 cm^{-1} and 804 cm^{-1} , respectively. The extra peak observed in Fig. 2 at 840 cm^{-1} is therefore consistent with extra oxygen being accommodated in the monoclinic PSZ structure through the formation of peroxide ions, that is, consistent with the experimental observation

indicating the presence of the monoclinic polymorph and the modelling prediction indicating the significant preference for excess oxygen to reside within the monoclinic polymorph.

To conclude: we have demonstrated through a combination of experiment and modelling methods that the accommodation of excess oxygen beyond the standard $(\text{ZrO}_2)_{1-x}(\text{Y}_2\text{O}_3)_{1/2-x}$ is plausible. The predicted enthalpy of solution suggests that the solubility of oxygen in the monoclinic structure is favourable, whilst solubility of oxygen into the tetragonal polymorph may proceed only once entropic factors are considered – both oxides forming the O_2^{2-} peroxide defect, supported by Raman spectra in this work. The Raman active stretching mode of this defect was predicted and shown consistent with experimental observations of the YSZ-8 which highlighted the formation of a new peak upon treatment in 30% H_2O_2 solution. Further work to corroborate this prediction could include NMR spectroscopy, carried out with oxygen-18 H_2O_2 solution and alternative oxidation routes. The impact of deviation in stoichiometry on the ionic conductivity in this material is of particular interest when considering its long-term efficiency and behaviour for fuel cell and related applications (it is not known whether the presence of the defect will aid or hinder ionic conductivity). The results may also play an interesting role in the mechanical degradation of yttria-doped zirconias, potentially stabilizing or accelerating the formation of the monoclinic phase (e.g. during so-called low temperature degradation LTD [19]).

Acknowledgements

This work was carried out as part of the Sêr Cymru II programme funded through the Welsh European Funding Office (WEFO) under the European Development Fund (ERDF). Computing resources were made available by HPC Wales and Supercomputing Wales. SCM would like to acknowledge the support of the members of the MUZIC-3 programme, particularly Magnus Limbäck, Antoine Claisse and Jonna Partezana.

References

- [1] K. Venkatesan, R. Ramanujam, P. Kuppan, *Procedia Eng.* 97 (2014) 1626–1636.
- [2] V. Stanic, et al., *Biomaterials* 23 (2002) 3833–3841.
- [3] D. Clarke, S. Phillpot, *Mater. Today* 8 (2005) 22–29.
- [4] D. Richerson, W. Lee, *Modern Ceramic Engineering*, 4th ed. CRC Press, 2018.
- [5] W. Lee, M. Rainforth, *Ceramic Microstructures: Property Control by Processing*, Chapman and Hall, 1994.
- [6] J. Kelly, I. Denry, *Dent. Mater.* 24 (2008) 289–298.
- [7] M. Zocate, L. Minervini, D. Bradfield, R. Grimes, K. Sickafus, *Solid State Ionics* 128 (2000) 243–254.
- [8] S. Skinner, J. Kilner, *Mater. Today* 6 (2003) 30–37.
- [9] S. Middleburgh, I. Karatchevtseva, B. Kennedy, P. Burr, Z.R.E. Zhang, R. Grimes, G. Lumpkin, *J. Mater. Chem. A* 2 (2014) 15883–15888.
- [10] S. Middleburgh, G. Lumpkin, R. Grimes, *Solid State Ionics* 253 (2013) 119–122.
- [11] L. J.H., X. Yang, K. Haller, J. Laane, G. Mestl, H. Knozinger, *J. Phys. Chem.* 97 (1993) 13810–13813.
- [12] S. Su, A. Bell, *Catal. Lett.* 36 (1996) 15–19.
- [13] M. Rushton, I. Ipatova, L. Evtits, W. Lee, S. Middleburgh, *RSC Adv.* 9 (2019) 16320–16327.
- [14] H. Toraya, M. Yoshimura, S. Somiya, *J. Am. Ceram. Soc.* 67 (1984) 119–122.
- [15] H. Zhou, J. Li, D. Yi, L. Xiao, *Phys. Proc.* 22 (2011) 14–19.
- [16] I. Gonzalo-Juan, B. Ferrari, M. Colomer, M. Rodriguez, A. Sanchez-Herencia, P.-Y. Koh, A. Teja, *Mater. Chem. Phys.* 134 (2012) 451–458.
- [17] E. Leib, U. Vainio, R. Pasquarelli, J. Kus, C. Czacskke, N. Walter, R. Janssen, M. Muller, A. Schryer, H. Weller, T. Vossmeier, *J. Colloid Interface Sci.* 448 (2015) 582–592.
- [18] C. Viazzi, J.-P. Bonino, F. Ansart, A. Barnabe, *J. Alloys Compd.* 452 (2008) 377–383.
- [19] J. Chevalier, L. Gremillard, *J. Am. Ceram. Soc.* 92 (2009) 1901–1920.
- [20] O. Fabrichnaya, F. Aldinger, *Z. Metallkd.* 95 (2004) 27–39.
- [21] S. Aruna, N. Balaji, K. Rajam, *Mater. Charact.* 62 (2011) 697–705.
- [22] L. Shi, K.-C. Tin, N.-W. Wong, *J. Mater. Sci.* 34 (1999) 3369–3374.
- [23] C. Kontoyannis, M. Orkoulas, *J. Mater. Sci.* 29 (1994) 5316–5320.
- [24] S. Venkateswaran, *Nature* 127 (1931) 406.
- [25] M. T., M.I.I.e.a. Lopez, *Chem. Eng. J.* 166 (2011) 1061–1065.
- [26] H.H. Eysel, S. Thym, *Z. Anorg. Allg. Chem.* 411 (1975) 97–102.
- [27] G. Kresse, J. Hafner, *Phys. Rev. B* 47 (1993).

- [28] G. Kresse, J. Hafner, Phys. Rev. B 49 (1994) 14251.
- [29] G. Kresse, J. Furthmüller, Comput. Mater. Sci. 6 (1996) 15–50.
- [30] G. Kresse, J. Furthmüller, Phys. Rev. B 54 (1996) 11169.
- [31] P.E. Blochl, Phys. Rev. B 50 (1994) 17953.
- [32] G. Kresse, D. Joubert, Phys. Rev. B 59 (1999) 1758.
- [33] J.P. Perdew, K. Burke, M. Ernzerhof, Phys. Rev. Lett. 77 (1996) 3865.
- [34] J.P. Perdew, K. Burke, M. Ernzerhof, Phys. Rev. Lett. 78 (1997) 1396.
- [35] A. Kushuma, B. Yildiz, J. Mater. Chem. 20 (2010) 4809–4819.
- [36] R. Devanathan, W. Weber, S. Singhal, J. Gale, Solid State Ionics 177 (2006) 1251–1258.
- [37] G. Stapper, M. Bernasconi, N. Nicoloso, M. Parrinello, Phys. Rev. B 59 (1999) 797.